Supplement of

Constraints on NO_x emission in Thailand using GEMS satellite data

Thongsame et al.

Correspondence to: Worapop Thongsame (t.worapop@gmail.com)

S1 The impact of the hyperparameter on IFDMB

In this section, we evaluate the impact of C_1 and C_2 parameters on the IFDMB performance. IFDMB with fixed diurnal update is applied to four different sets of $[C_1, C_2]$ parameters, and we evaluate IFDMB solution as a function of iteration for each. The four $[C_1, C_2]$ parameters are [2x10^{15},1], [2x10^{15},10], [1x10^{14},1], and [1x10^{14},10]. We find that iteration five is the optimal iteration for [2x10^{15},1] and [2x10^{15},10], and iteration two is optimal for [1x10^{14},1] and [1x10^{14},10]. All four parameters produce similar spatial patterns in model performance (Table S1). The IFDMB with fixed diurnal update significantly reduces both NMB and NRMSE relative to GEMS observations across Thailand, particularly in the Bangkok Metropolitan Region.

Increasing C_1 from 1x10^{14} to 2x10^{15} molecules cm^{-2} suppresses the influence of satellite constraints, resulting in higher NMB and NRMSE values for the [2x10^{15},1] and [2x10^{15},10] cases, especially in Central and East Thailand (Figs. S1 and S2). This is attributed to smaller emission updates under high C_1. Even though the σ_o in these regions is low (on the order of 0.5 - 0.2 x 10^{13} molecules cm^{-2}), the corresponding NO_2 VCDs are also relatively low, which leads to a small $J_{prediction}$ compared to the $J_{parameter}$. This causes the solution to remain close to the prior emissions. However, a larger C_1 value helps prevent overfitting in rural North Thailand, where σ_o is much higher.

Increasing C_2 from 1 to 10 mol km^{-2} hr^{-1} has minimal impact in the [1x10^{14},1] and [1x10^{14},10] cases. While the percentage change in emissions is relatively larger in [1x10^{14},10], the improvements in NMB and NRMSE are comparable: [1x10^{14},1] reduces NMB by 66% and NRMSE by 62%, whereas [1x10^{14},10] achieves 47% and 48% reductions, respectively (Table S1). This is because the larger emission adjustments occur in low-emission areas, thus contributing little to the overall NO_2 VCD improvements. In contrast, the effect of increasing C_2 is more pronounced in the [2x10^{15},1] and [2x10^{15},10] cases. A higher C_2 value (10 mol km^{-2} hr^{-1}) allows emissions in Central and East Thailand to be more effectively constrained by GEMS data compared to C_2 = 1 (Figs. S1 and S2). Consequently, NMB and NRMSE improve significantly in 2x10^{15},1] with ~30% reduction. The [2x10^{15},10] yields reductions of approximately 47% in both metrics.

The parameter C_1 notably influences the relative errors between the Bangkok Metropolitan Region and North Thailand. A low C_1 value (1×10^{14} molecules cm^{-2}) permits large adjustments even in high error areas (Fig. S3) in GEMS like North Thailand. This greatly decreases NMB and RMSE in the Bangkok Metropolitan Region, but also excessively increases bias and error in North Thailand (Figs. S1 and S2). In contrast, a high C_1 (2×10^{15} molecules cm^{-2}) constrains adjustments in the North, preventing over-correction and lowering bias and error in that region. However, it also limits the improvement in the Bangkok Metropolitan Region.

The second parameter, C_2, primarily affects adjustments for smaller emission sources (such as rural areas). Using a smaller C_2 limits the changes in rural emissions (Fig. S3), keeping those values closer to the prior and yielding lower bias and error against TROPOMI. In contrast, a larger C_2 allows greater adjustments for low-emission areas, which led to higher bias and error

in rural North due to overfitting to the GEMS data. Overall, the adjustable parameters $[C_1, C_2]$ in IFDMB offer flexibility to manage the mismatch between GEMS and TROPOMI in the North by moderating the influence of emission updates in high-error regions and balancing between prior and posterior estimates.

Table S1: Monthly statistical evaluation between WRF-Chem and GEMS NO_2 VCD of IFDMB for each $[C_1, C_2]$ parameters: [1x10^{14}, 1], [2x10^{15}, 1], [1x10^{14}, 10], and [2x10^{15}, 10].

	[1 x 1014, 1]			[2 x 1015, 1]			[1 x 1014, 10]			[2 x 1015, 10]		
	MB	RMSE	*R*	MB	RMSE	*R*	MB	RMSE	*R*	MB	RMSE	*R*
All hour	28.78	58.01	0.83	58.95	106.51	0.67	31.90	56.25	0.84	44.12	78.38	0.80
8 AM	182.35	238.83	0.74	239.49	320.79	0.56	184.21	235.57	0.75	207.88	266.08	0.72
9 AM	137.07	186.46	0.81	191.50	268.58	0.69	142.48	187.51	0.80	163.54	215.74	0.81
10 AM	68.16	116.39	0.80	109.21	179.89	0.69	74.24	117.91	0.78	89.83	142.27	0.79
11 AM	22.23	67.94	0.77	51.59	112.94	0.63	26.71	67.61	0.77	38.56	87.41	0.75
12 PM	-3.62	50.73	0.72	19.85	84.19	0.55	-0.24	48.86	0.73	9.10	66.10	0.69
2 PM	-6.81	56.53	0.65	16.52	90.37	0.48	-4.75	53.50	0.68	5.78	73.10	0.61
3 PM	2.28	59.95	0.66	27.87	98.65	0.51	5.07	58.27	0.69	15.69	78.92	0.63

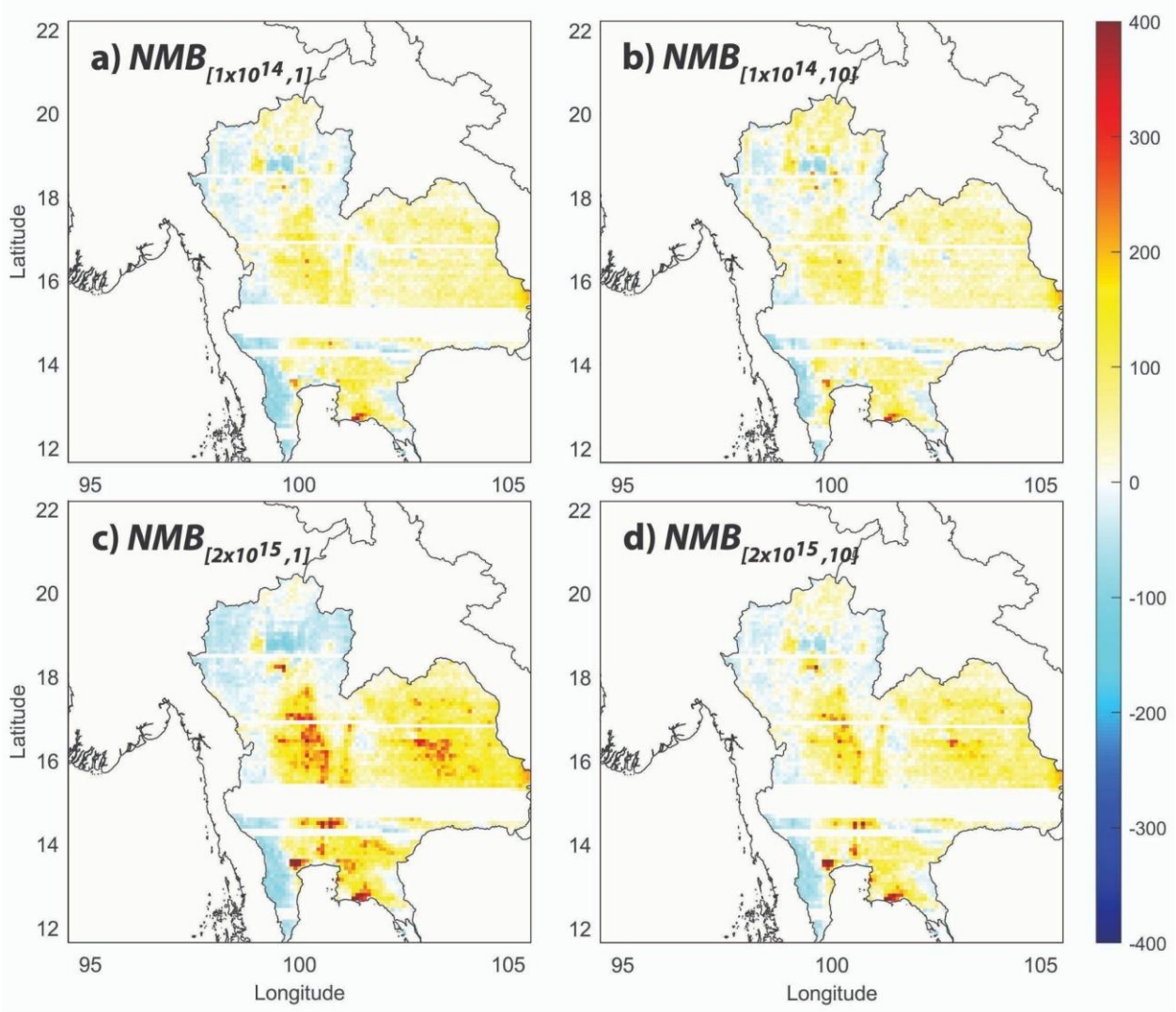

Figure S1: Normalized Mean Bias (NMB) of hourly NO_2 VCD between WRF-Chem and GEMS of IFDMB for September 2023 using $[C_1, C_2]$: (a) [1x10^{14}, 1], (b) [1x10^{14}, 10], (c) [2x10^{15}, 1], and (d) [2x10^{15}, 10].

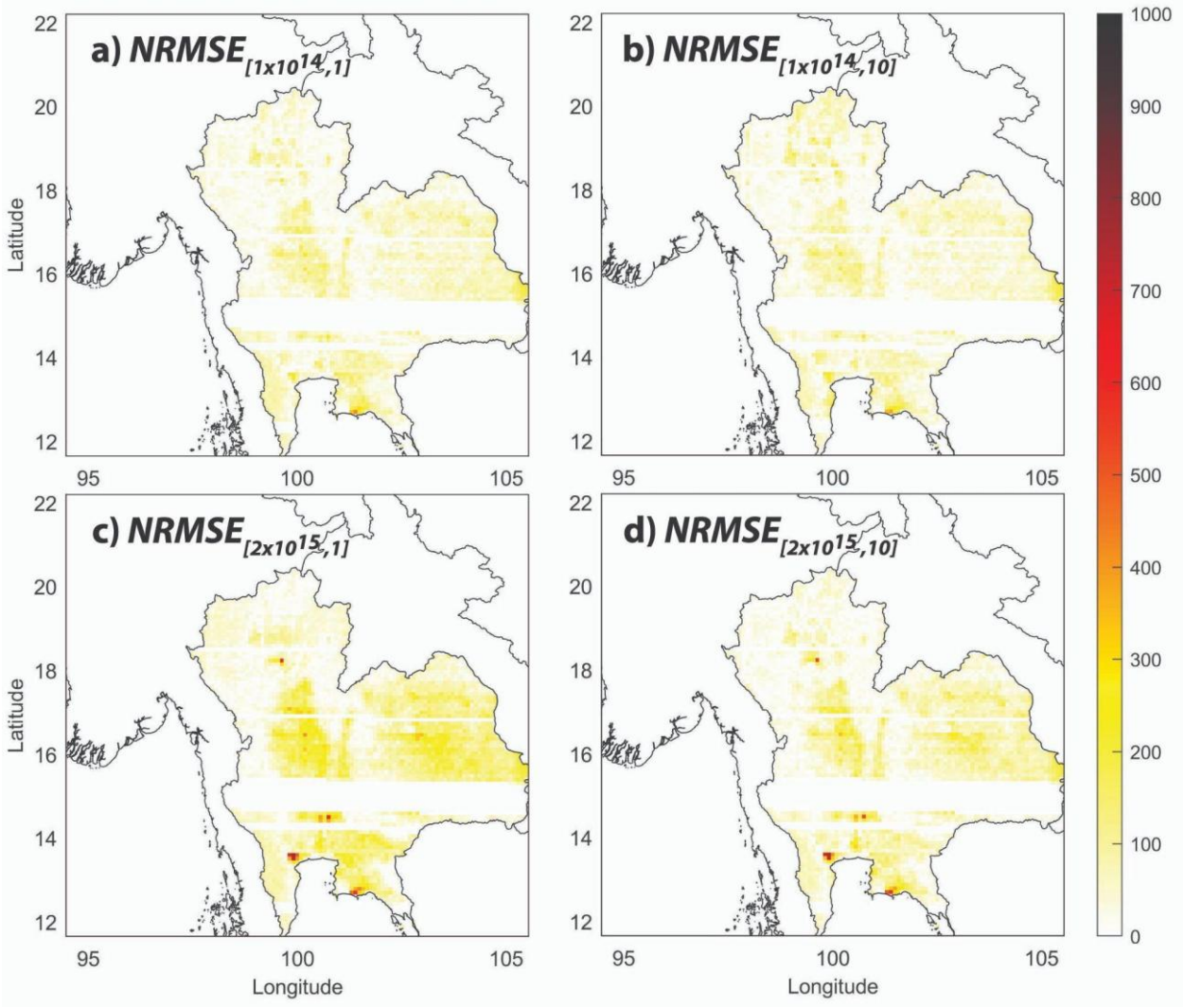

Figure S2: Normalized Root Mean Square (NRMSE) of hourly NO_2 VCD between WRF-Chem and GEMS of IFDMB for September 2023 using $[C_1, C_2]$: (a) [1x10^{14}, 1], (b) [1x10^{14}, 10], (c) [2x10^{15}, 1], and (d) [2x10^{15}, 10].

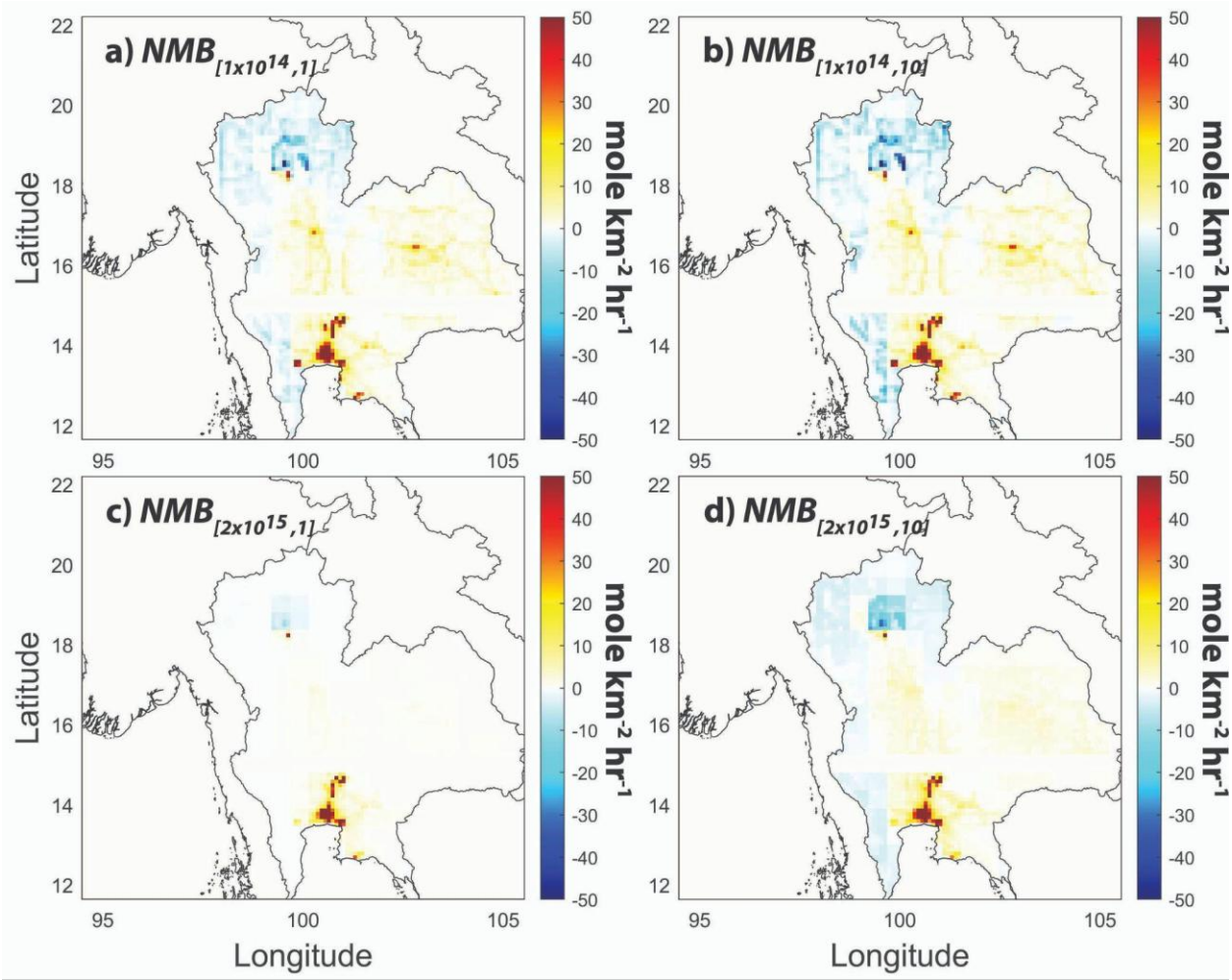

Figure S3: The emission changes from prior for IFDMB with different $[C_1, C_2]$ values: (a) changes from [1x10^{14}, 1], (b) changes from [1x10^{14}, 10], (c) changes from [2x10^{15}, 1], and (d) changes from [2x10^{15}, 10].

S2 The comparison between GEMS DVCF and GEMS DOAS

The retrieval algorithm impacts the NO_2 VCDs from the GEMS satellite. Yang et al. (2023) use the Direct Vertical Column Fitting (DVCF) algorithm, whereas GEMS version 3 relies on the DOAS algorithm. The two products also differ in their prior models. The DVCF algorithm (Huang et al., 2022; Yang et al., 2014) finds the modeled radiance spectra (I_{TOA}) that match the satellite measured spectra (I_m) by minimizing the cost function as shown in Eq (S1).

$$\ln I_m(\lambda) - \ln I_{TOA}(\lambda) = V \int_0^{\infty} \frac{\partial \ln I_{TOA}(\lambda)}{\partial \tau_z} S_z \sigma(\lambda, T_z) dz - \sum_{i=1}^{m} \xi_i \sigma_i(\lambda, T_i) + \sum_{k=0}^{n=1} \frac{\partial \ln I_{TOA}(\lambda)}{\partial R} \Delta R_k (\lambda - \lambda_0)^k + \varepsilon \quad \text{(S1)}$$

where λ is the wavelength and V is the NO_2 vertical column. S_z is the shape factor derived from the normalized vertical profile at the altitude (z). A more detailed explanation of the algorithm is in Yang et al. (2014).

The prior model used in GEMS DVCF is GEOS-CF using the HTAP inventory, while that in GEMS DOAS is GEOS-Chem using the ASIA-AQv3 inventory. These differences contribute to variations in the slant columns, vertical columns, and averaging kernels between GEMS DVCF and GEMS DOAS.

Because the averaging kernels differ between GEMS DVCF and GEMS DOAS, direct comparison is not feasible; therefore, we assess the relative NO_2 distributions instead. GEMS DVCF has relatively higher NO_2 over the Bangkok Metropolitan Region compared to North Thailand, while GEMS DOAS has higher NO_2 levels in the North (Fig. S4). Notably, GEMS DOAS has a large NO_2 signal over Lampang due to the high NO_x emissions in ASIA-AQv3. This high NO_2 is absent in both GEMS DOAS and TROPOMI. The uncertainties in ASIA-AQv3 lead to high retrieval error in GEMS DOAS in Lampang. Furthermore, both GEMS ACX and GEMS v3 exhibit artificial striping, implying that the stripes originate from the instrument itself rather than the retrieval algorithm.

We also compare the magnitude of NO_2 columns between the two retrievals using the baseline WRF-Chem simulation as a reference. When compared with GEMS DOAS, the baseline simulation generally overestimates NO_2 VCDs across Thailand, with an NMB of 84 and an NRMSE of 152 (Fig. S5). The model notably overestimates NO_2 in the Bangkok Metropolitan Region but underestimates it in North and West Thailand. For GEMS DVCF, we normalize the bias and error using the retrieval error from GEMS DOAS, as there is no error provided in GEMS DVCF. The baseline simulation overestimates NO_2 VCDs across most of the domain, with an NMB of 198 and NRMSE of 216, except in the western Bangkok Metropolitan Region (Fig. S5). This suggests that the CAMS-GLOB-ANT inventory overestimates NO_x emissions in Thailand when compared with GEMS DOAS. In contrast, CAMS-GLOB-ANT tends to underestimate NO_x emissions in North Thailand relative to GEMS DOAS. Although GEMS DVCF shows good agreement with CAMS-GLOB-ANT over major NO_x sources such as Bangkok, Rayong, and the Mae Moh power plant, it yields much lower NO_2 VCDs in small cities

and background regions compared to these urban and industrial areas. Additionally, GEMS DVCF shows a broader spatial spread of NO_2 over the Bangkok Metropolitan Region than TROPOMI. Considering these characteristics, we adopt the GEMS DOAS product for this study.

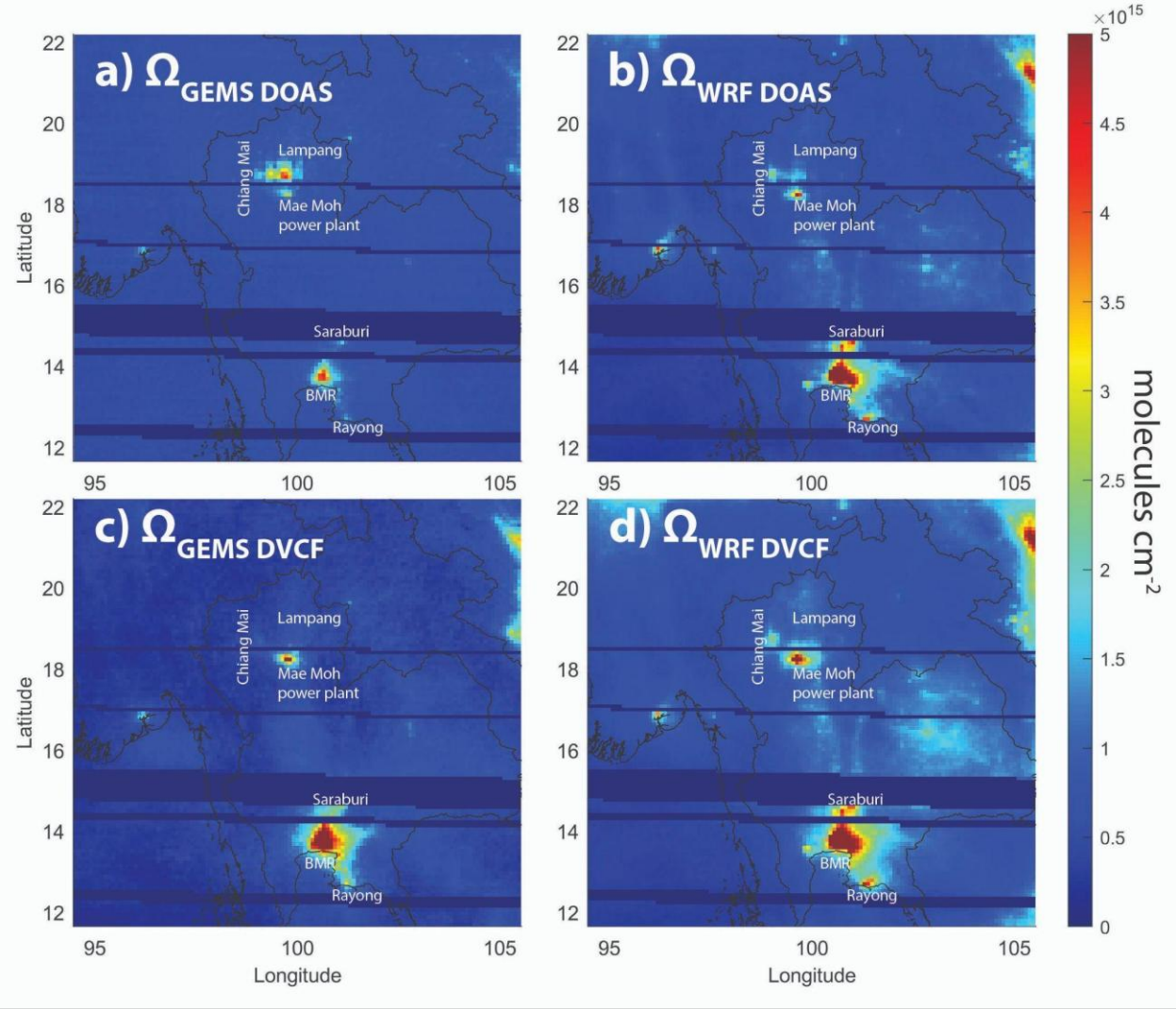

Figure S4: Monthly average tropospheric NO_2 VCD in September 2023 from GEMS DOAS (a) and GEMS DVCF (c), the baseline simulation applying the averaging kernel from GEMS DOAS (b) and GEMS DVCF (d). High NO_2 VCDs are observed over urban areas such as Chiang Mai, Lampang, and the Bangkok Metropolitan Region (BMR), as well as over the Mae Moh power plant and industrial zones in Saraburi and Rayong.

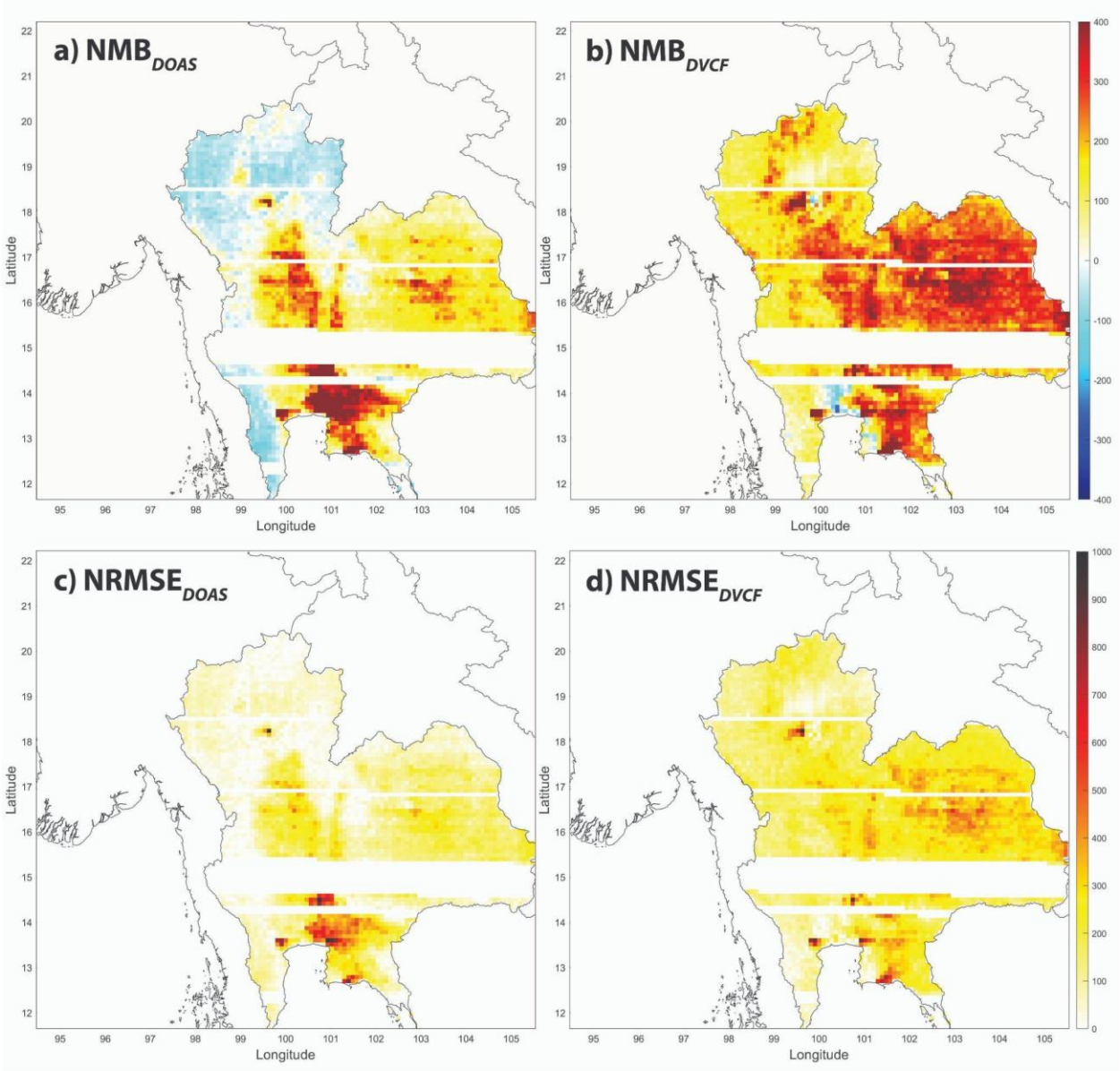

Figure S5: Normalized Mean Bias (NMB) of NO_2 VCD between the baseline simulation and GEMS DOAS (a) and GEMS DVCF (b). Normalized Root Mean Square Error (NRMSE) of NO_2 VCD between the baseline simulation and GEMS DOAS (c) and GEMS DVCF (d).

S3 Uncertainty in GEMS DOAS due to ASIA-AQv3 Emission Inventory

According to the GEMS DOAS team (private communication), the operational GEMS version 3 uses the ASIA-AQv3 anthropogenic emissions inventory as input for its prior GEOS-Chem model. This prior is used to derive key retrieval parameters, including air mass factors, shape factors, and averaging kernels. In our study period (September 2023), biomass burning in Thailand is minimal (late wet season), so anthropogenic emissions are the dominant source of NO_2. Consequently, the ASIA-AQv3 inventory can exert a significant influence on the retrieved GEMS NO_2 VCDs over Thailand during this time.

We discovered that the ASIA-AQv3 inventory contains an anomalously high NO_x point source in Lampang. The magnitude of this single source in ASIA-AQv3 is significantly larger than the NO_x emissions allocated to known major sources like the Mae Moh power plant or even the Bangkok Metropolitan Region, within the same inventory. This large Lampang emission does not appear in the CAMS or the HTAP global inventories (Fig. S6), and there are no known large power plants or industrial facilities in Lampang city that would justify such a high emission. Notably, the total NO_x emissions for Thailand in ASIA-AQv3 are of the same order as those in CAMS and HTAP, implying that the Lampang point source significantly contributes to total NOx emissions in Thailand. In other inventories, by contrast, the Bangkok Metropolitan Region and the Mae Moh power plant are the main NOx contributors. This suggests that ASIA-AQv3's Lampang point source might be too high for NOx emissions in Thailand.

Our inversion results indicate that ASIA-AQv3 indirectly affects the top-down emission estimates. The IFDMB posterior NOx emissions for North Thailand appear to be influenced by the Lampang point source (Fig. S7). Because our WRF-Chem model and GEMS data are aggregated onto a coarse grid (~81 × 81 km^2), any extreme point source signal in the GEMS observations tends to be spatially spread out over the surrounding area. As a result, the influence of the Lampang point source can be seen in the posterior emission field over a broad area of North Thailand. However, since we did not use ASIA-AQv3 directly to adjust the emissions, the posterior emissions do not simply replicate the ASIA-AQv3 spatial pattern.

Furthermore, the GEMS retrieval reported high RMSE for NO_2 VCDs in the area around this Lampang point source. In future applications of GEMS data, we recommend filtering the satellite data not only by the standard quality flags but also by excluding data points with abnormally high errors. This is because the RMSE (order of 10^{13}) in GEMS version 3 is relatively low compared to the NO_2 VCDs (order of 10^{15}). Consequently, the weighting by σ in the cost function is insufficient to handle this uncertainty. Applying such an error filter would help remove spurious signals and improve the robustness of emission updates derived from GEMS satellite observations.

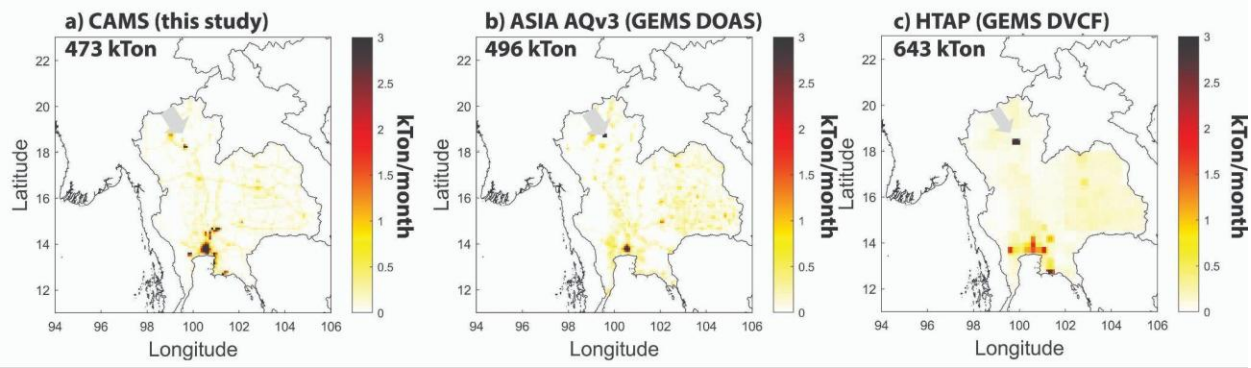

Figure S6: The comparison of NO_x emissions during September 2023 from three different inventories: a) CAMS, b) ASIA AQv3, and c) HTAP. The arrow points to the high NO_2 VCDs in GEMS DOAS.

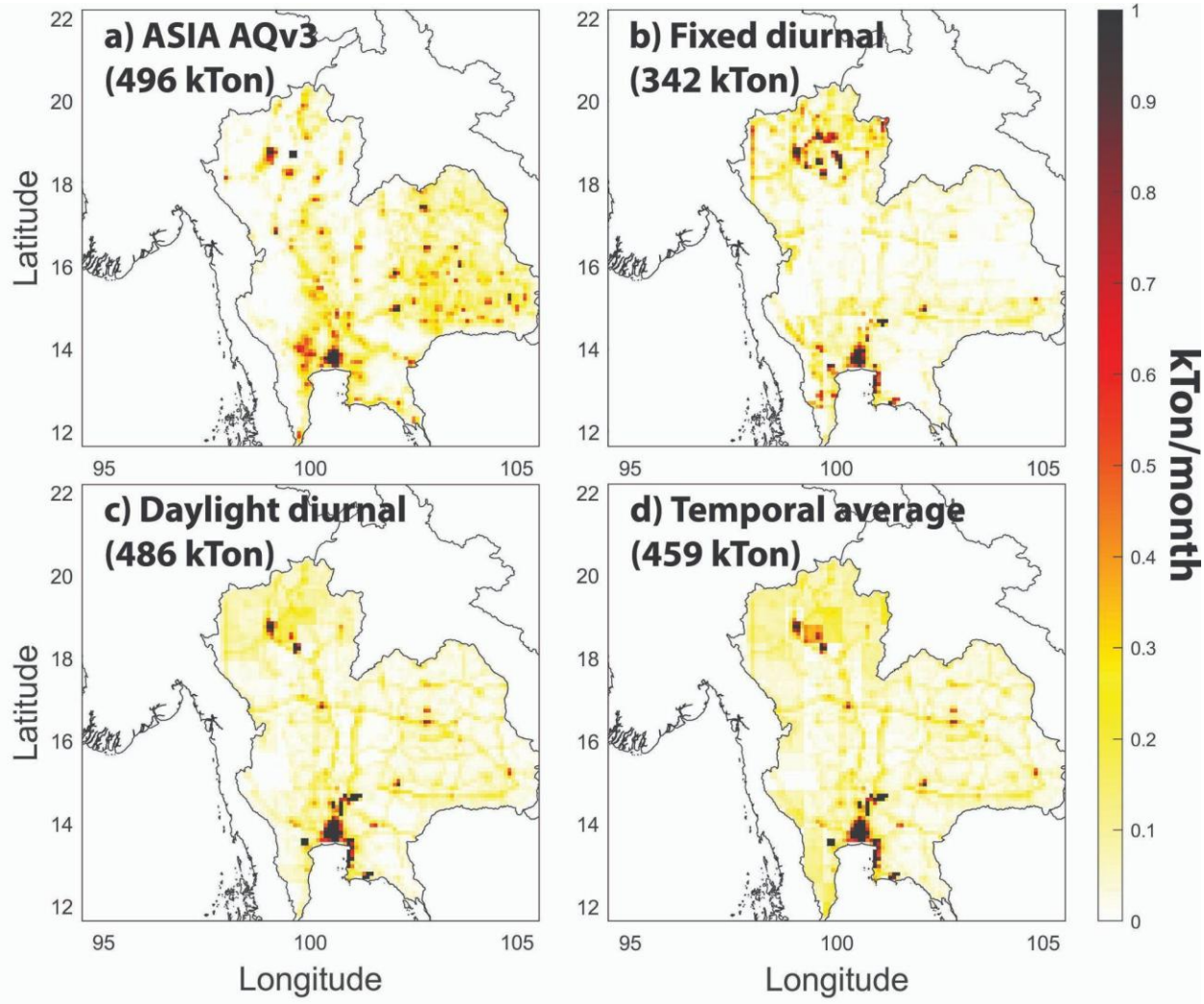

Figure S7: The comparison of NO_x emissions between ASIA AQv3 and our posterior emissions in September 2023.

Supplement figures

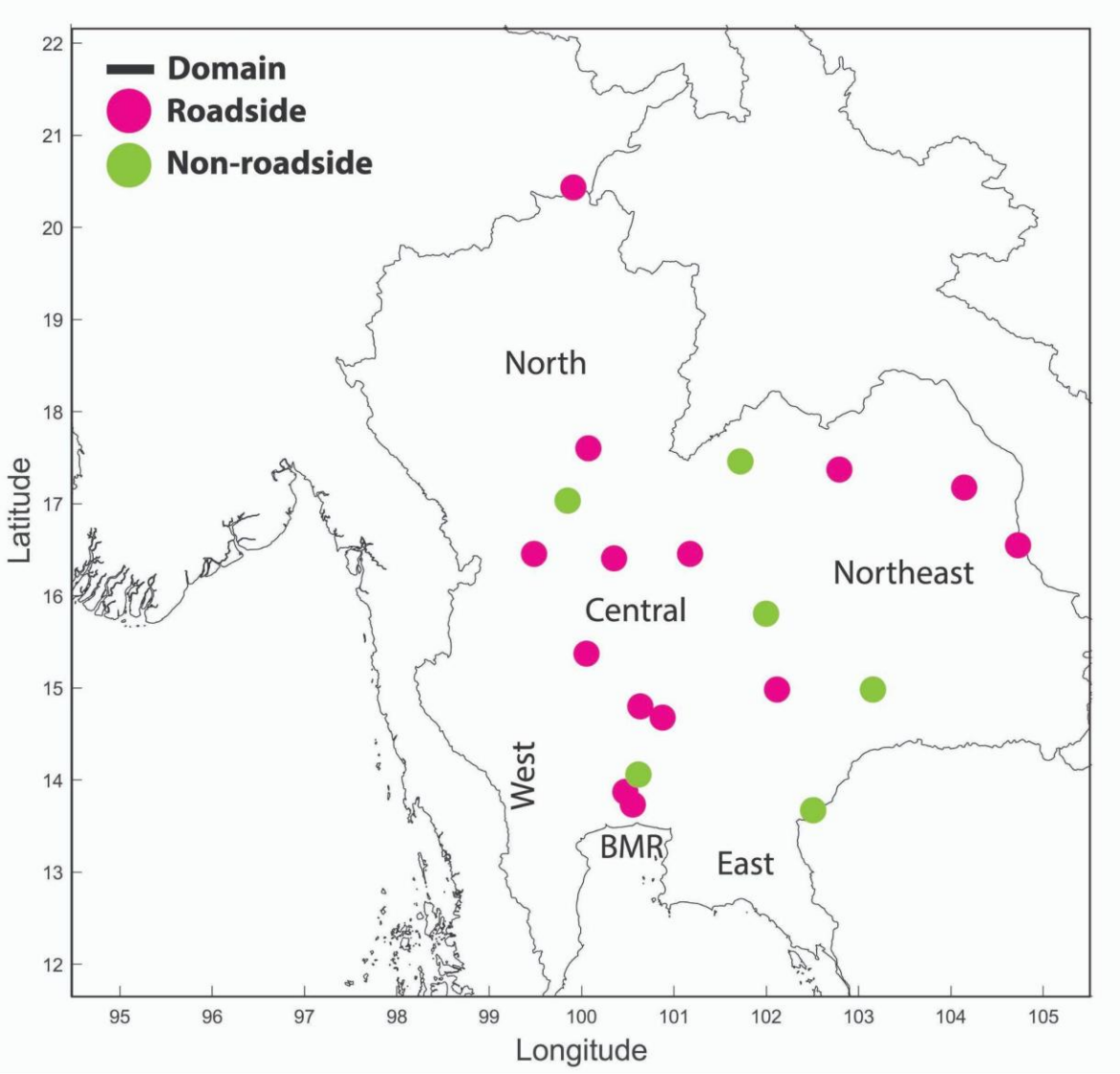

Figure S8: Model domain and location of PCD stations, classified as roadside (pink) and non-roadside (green). BMR is the Bangkok Metropolitan Region.

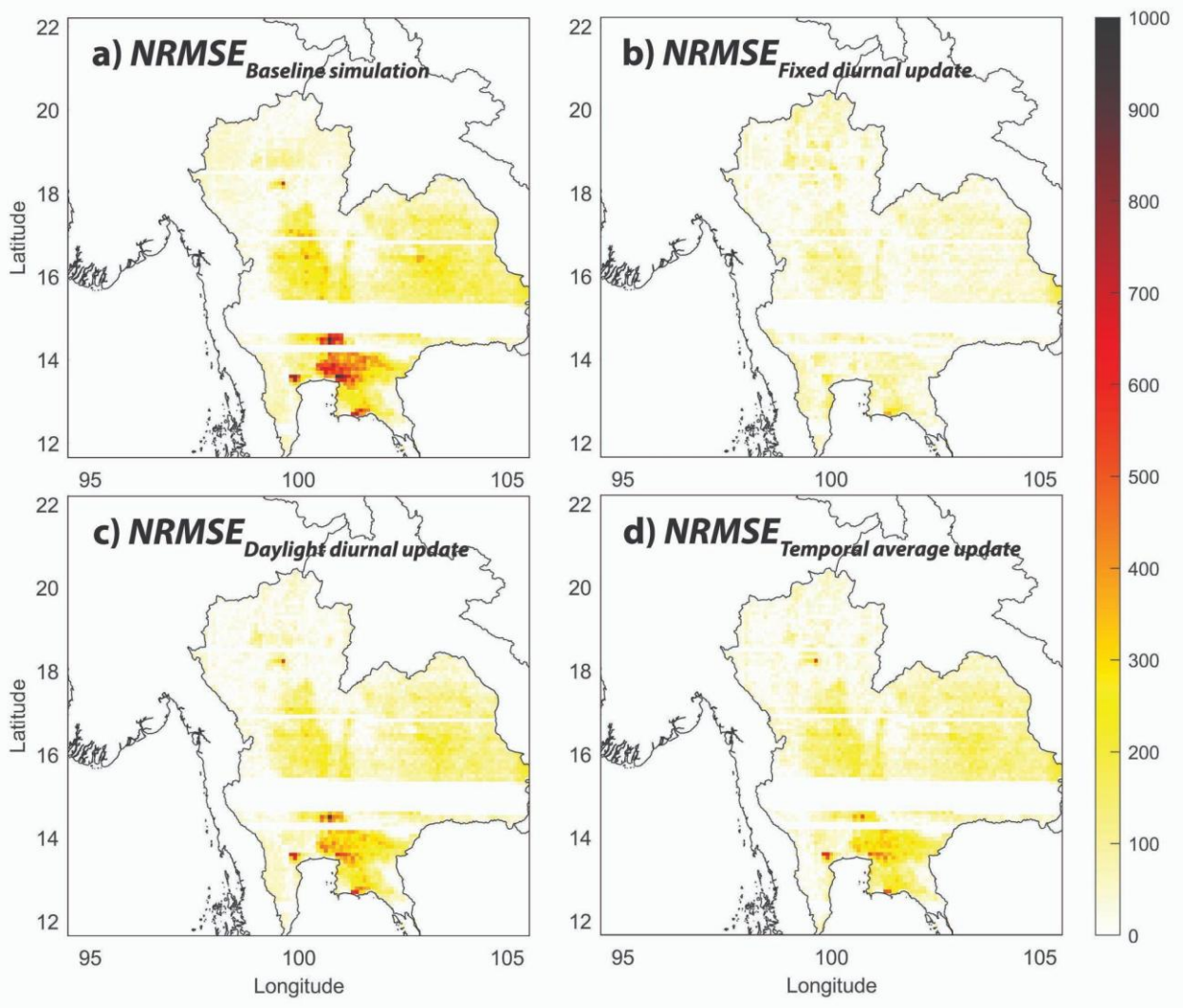

Figure S9: Normalized Root Mean Square (NRMSE) of NO_2 VCD between WRF-Chem and GEMS of IFDMB for September 2023 using (a) prior emissions, and emissions updated by (b) fixed diurnal, (c) daylight diurnal, and (d) temporal average update schemes.

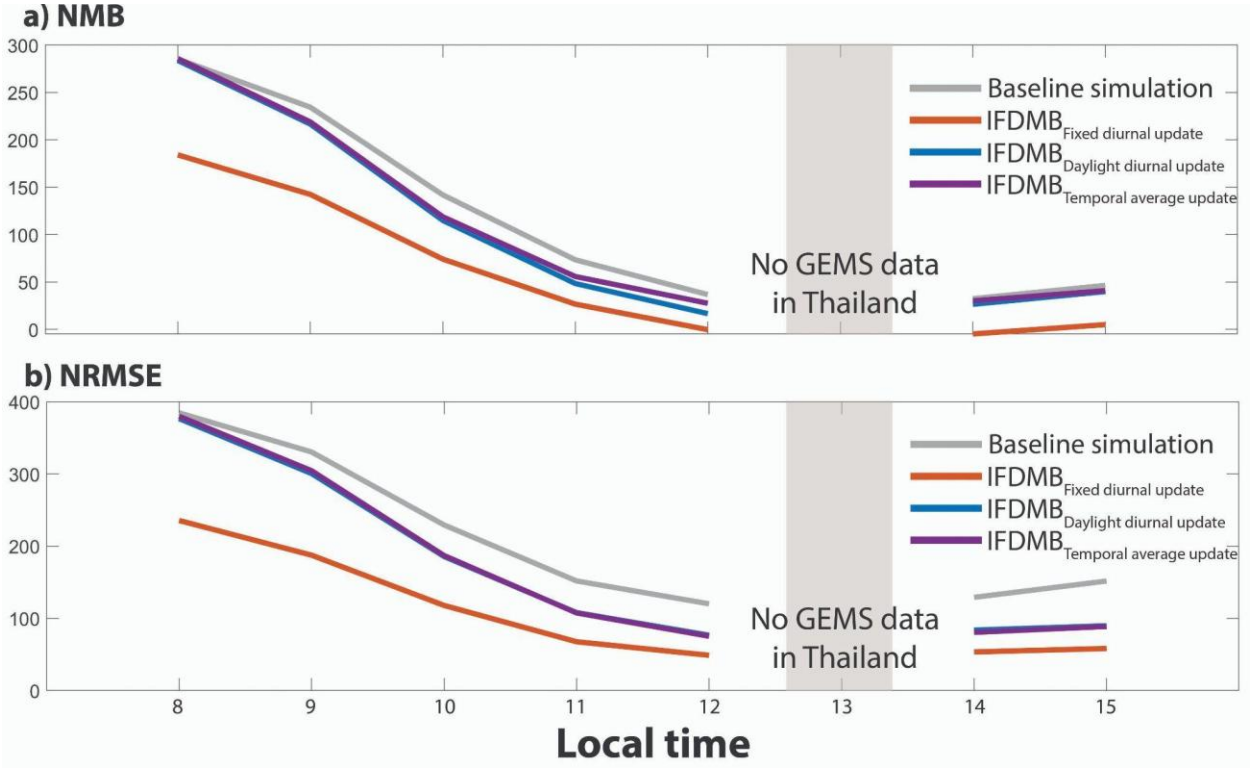

Figure S10: Monthly statistical evaluation between WRF-Chem and GEMS NO_2 VCD of each hour averaged from Thailand grid cells.

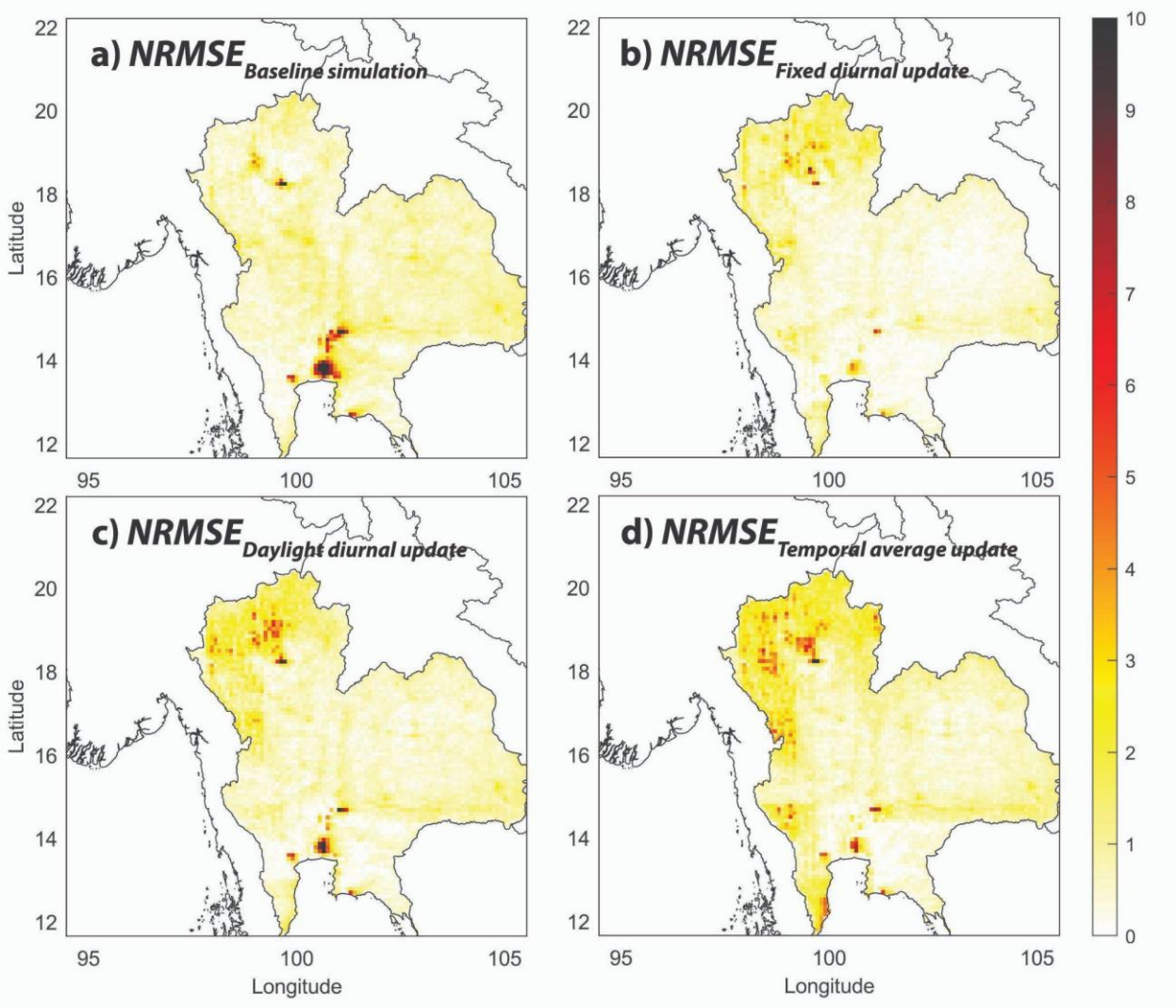

Figure S11: NRMSE of NO_2 VCD between WRF-Chem and GEMS of IFDMB for September 2023 using (a) prior emissions, and emissions updated by (b) fixed diurnal, (c) daylight diurnal, and (d) temporal average update schemes.

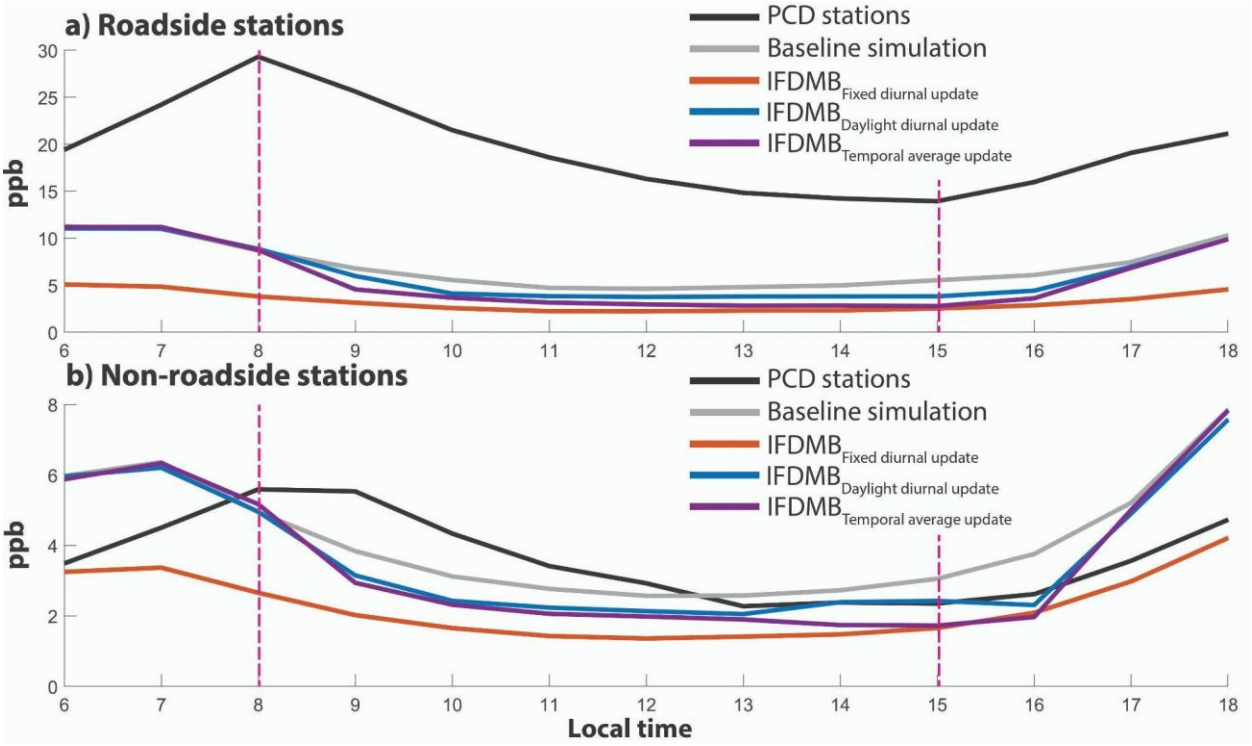

Figure S12: The monthly average diurnal profile of surface NO_x mixing ratios from PCD stations (black) and WRF-Chem: the baseline simulation (gray), IFDMB with fixed diurnal update (orange), IFDMB with daylight diurnal update (blue), and IFDMB with temporal average update (purple). PCD stations are classified into roadside stations (a) and non-roadside stations (b). The pink lines mark the GEMS overpass times in Thailand from 08:00 - 15:00 local time.

Supplement table

Table S2: Monthly statistical evaluation between TROPOMI NO_2 VCD and WRF-Chem for IFDMB with different update schemes for Thailand and BMR.

Thailand	**NMB (unitless)**	**NRMSE (unitless)**	***R***
Baseline simulation	0.80	1.21	0.79
$IFDMB_{Fixed\ diurnal}$	0.60	0.86	0.61
$IFDMB_{Daylight\ diurnal}$	0.84	1.19	0.63
$IFDMB_{Temporal\ average}$	1.05	1.41	0.47
BMR	**NMB (unitless)**	**NRMSE (unitless)**	***R***
Baseline simulation	3.46	5.26	0.90
$IFDMB_{Fixed\ diurnal}$	0.59	1.25	0.93
$IFDMB_{Daylight\ diurnal}$	1.58	3.22	0.88
$IFDMB_{Temporal\ average}$	0.66	2.05	0.82

References

Huang, X., Yang, K., Kondragunta, S., Wei, Z., Valin, L., Szykman, J., and Goldberg, M.: NO2 retrievals from NOAA-20 OMPS: Algorithm, evaluation, and observations of drastic changes during COVID-19, Atmos. Environ., 290, 119367, https://doi.org/10.1016/j.atmosenv.2022.119367, 2022.

Yang, K., Carn, S. A., Ge, C., Wang, J., and Dickerson, R. R.: Advancing measurements of tropospheric NO_2 from space: New algorithm and first global results from OMPS, Geophys. Res. Lett., 41, 4777–4786, https://doi.org/10.1002/2014GL060136, 2014.

Yang, K., Kondragunta, S., and Wei, Z.: The NO 2 Algorithm for GeoXO-ACX and Application to GEMS and TEMPO, https://doi.org/10.22541/essoar.170365312.22362491/v1, 2023.